Electrical resistivity tomography applied to geological, hydrogeological and engineering investigations at a former waste disposal site

(Shortened form of title: Resistivity imaging of waste)

Jonathan E. Chambers[1*], Oliver Kuras[1], Philip I. Meldrum[1], Richard D. Ogilvy[1], and

Jonathan Hollands[2]

Final (Third) Revision

Date of submission: 22nd June 2006

[1] British Geological Survey, Keyworth, Nottingham, NG12 5GG, UK
[2] North Lanarkshire Council, Fleming House, 2 Tryst Road, Cumbernauld, G67 1JW, UK
* Corresponding Author. Fax: +44 115 936 3261. E-Mail Address: jecha@bgs.ac.uk (J. E. Chambers).

1

ABSTRACT

A former dolerite quarry and landfill site was investigated using 2D and 3D electrical resistivity tomography (ERT), with the aims of determining buried quarry geometry, mapping bedrock contamination arising from the landfill, and characterizing site geology. Resistivity data were collected from a network of intersecting survey lines using a Wenner-based array configuration. Inversion of the data was carried out using 2D and 3D regularized least-squares optimization methods with robust (L1-norm) model constraints. For this site, where high resistivity contrasts were present, robust model constraints produced a more accurate recovery of subsurface structures when compared to the use of smooth (L2-norm) constraints. Integrated 3D spatial analysis of the ERT and conventional site investigation data was shown in this case to provide a highly effective means of characterizing the landfill and its environs. The 3D resistivity model was successfully used to confirm the position of the landfill boundaries, which appeared as electrically well-defined features that corresponded extremely closely to both historic maps and intrusive site investigation data. A potential zone of leachate migration from the landfill was identified from the electrical models; the location of this zone was consistent with the predicted direction of groundwater flow across the site. Unquarried areas of a dolerite sill were imaged as a resistive sheet-like feature, whilst the fault zone appeared in the 2D resistivity model as a dipping structure defined by contrasting bedrock resistivities.

INTRODUCTION

Electrical resistivity tomography (ERT) is now a well-established tool for environmental and engineering site investigation, and is routinely applied to the detection of pollution (Daily et al., 1998; Goes and Meekes, 2004), the characterization of geological (Meads et al., 2003) and engineered structures (Daily and Ramirez, 2000), and hydrogeological studies (Binley et al., 2002; Sandberg et al., 2002). The great strengths of ERT are that it provides a relatively low cost, non-invasive and rapid means of generating spatial models of physical properties of the subsurface. It is especially beneficial for contaminated land investigations where it is generally desirable to minimize ground disturbance. A category of environmental and engineering problems for which ERT has proved to be particularly useful is the investigation of landfill sites, where it has been used to map landfill geometry (Reynolds and Taylor, 1996; Bernstone and Dahlin, 1997) and compositional variations (Yuval and Oldenburg, 1996; Bernstone et al., 2000; Guerin et al., 2004), and to detect bedrock contamination (Aristodemou and Thomas-Betts, 2000; Yoon et al., 2003; Abu-Zeid et al., 2004; Naudet et al., 2004). Most published studies have detailed the application of 2D ERT to landfill investigation; however, given that waste deposits are typically highly heterogeneous, full 3D solutions are often preferable (Chambers et al., 1999; Ogilvy et al., 1999; Dahlin et al., 2002; Ogilvy et al., 2002; Chambers et al., 2005).

Landfill sites are ubiquitous across the industrialized world, and represent a legacy going back many decades (e.g., Walsh and LaFleur, 1995). Although most modern landfill sites are carefully selected and engineered to minimize the potential for bedrock and groundwater contamination (e.g., USEPA, 1993; EU, 1999), there are huge numbers of sites that were developed before the hazards associated with waste disposal (Williams, 1991) were well understood. Consequently, many older landfill locations were chosen on

the basis of convenience and their proximity to the waste source, rather than environmental, geological or engineering considerations, and in many cases former minerals workings were used as they provided ready made voids in which to deposit waste (Williams, 1999).

Study objectives

In this study both 2D and 3D ERT were applied to the investigation of a former quarry and waste disposal site. The study site is an example of a UK waste disposal facility that began operating prior to 1ˢᵗ January 1976, at which time legislation controlling landfill operations came into effect in the form of the Control of Pollution Act (Great Britain, 1974). This site is therefore similar to hundreds of other landfill sites around the UK dating from this time, for which there were few controls on the tipping of waste, and no requirements to keep records of waste disposal or to engineer sites in such a way as to reduce the potential for the spread of pollution.

The principal objectives of the electrical surveys were to accurately define the northerly and westerly edges of the landfill, i.e., the boundaries of the former quarry, to assist in the planning of a proposed development adjacent to the site, and to provide information relating to landfill depth. Secondary objectives included the identification of potential pollution pathways from the landfill associated with the lack of an engineered barrier, and the characterization of site geology.

Site description

The site comprises a former dolerite quarry, which during the 1970s was in-filled with domestic waste and inert materials, and capped with clay. The area known to include the landfill site is disused, though much of the surrounding land has until recently been used

for agriculture. The site is dominated by grassland and marsh, though areas of dense vegetation and woodland are present in the north, and across the southwestern side. A marked topographic feature defining low ground to the south, which is likely to be associated with the northern limit of the dolerite sill, extends along the northwestern and northeastern edges of the site. In addition, an embankment running in a northwesterly direction is located within the site. This feature is characterized by a sharp change in slope, and defines an area of high ground to the northeast, which is thought to contain the landfill. It is likely that the sharp change in slope represents the limit of quarry spoil deposited in the area to the west of the former quarry.

Intrusive site investigation

In addition to the ERT surveys, three phases of intrusive investigations have been undertaken. The first (I) was carried out prior to the ERT surveys, and was very limited, comprising only a few sample locations (e.g., Figures 1 and 2, CP10, R01 and R02). The second intrusive investigation (II), which was focused on the fields adjacent to the quarry to the north and west, was carried out approximately 2 months after the ERT surveys, and was more extensive (e.g., Figures 1 and 2, BH50 to BH67). The final phase (III) was carried out approximately 11 months after the ERT surveys, and involved sample locations in and immediately adjacent to the quarry (Figures 1a and 2, BH01 to BH13). The phase III investigation confirmed that a mixture of domestic and inert wastes were contained in the landfill. Other information relating to the site included historic Ordnance Survey (OS) maps showing the extent of quarrying during the 1950s after the point at which quarrying was thought to have ceased.

Geology and hydrogeology

The landfill is situated within a quartz dolerite sill, which forms part of the late Carboniferous Midland Valley sill complex (Francis, 1982). Borehole records (i.e., BH60) from the site show a maximum sill thickness of 12.6 m. The sill has been partially excavated during quarrying operations, which in places extended to the base of the sill (e.g., BH05, BH06, BH07B and BH08). The sill was intruded into the Upper Limestone Formation (Cameron and Stephenson, 1985), which consists principally of coal-cyclic sequences that have been widely replaced by erosive sandstones. Intrusive records in this area have shown that the Upper Limestone Formation comprises mudstones, siltstones, sandstones and occasional thin coal bands.

The northern tip of the site is cut by an east-west trending fault, which is downthrown to the south. Consequently, the Upper Limestone strata to the north of the site are likely to be older that those underlying the landfill.

Drift deposits directly associated with the landfill have been removed by quarrying, and, likewise, trial pit and borehole records indicate that deposits are thin or absent in the area directly to the west of the landfill. However, Quaternary tills are present directly to the south and east of the site, and glaciofluvial sand and gravel drift deposits extend from its northern limits.

Intrusive investigations have revealed a shallow water table across the site, typically less than 3 m below ground level (bgl), which broadly follows the topography. A Kriged groundwater surface for the area was calculated using a 2.5 m surface grid from water levels observed during the phase II intrusive investigation (Figures 1b and 2). Data from phase II were used as they were collected shortly after the ERT surveys, and represented the widest distribution of sample points. Though none of the sample points were located within the quarry, the distribution of points did allow the regional hydraulic gradient in a broad area around the quarry to be considered.

DATA AQUISITION, INTERPRETATION AND DISPLAY

Survey strategy

The 3D electrical survey covered a rectangular area, along the western boundary of the landfill. The area was chosen to maximize coverage of the central, northern and western regions of the landfill. Dense vegetation, steep slopes and other physical impediments limited further extension of the survey to the north and east. In accordance with the local coordinate system adopted for this site, which is shown in red in Figure 1, the survey area extends from 0 to 155 m NE (x-axis) and from 0 to 210 m NW (y-axis). Elevations referred to in this paper are related to an arbitrary site datum.

The survey comprised 15 lines orientated parallel to the x-axis, positioned at 15 m intervals from 0 m NW to 210 m NW. In addition, data were collected from 4 tie lines orientated parallel to the y-axis, located at 30, 80, 120 and 155 m NE respectively. The tie lines were included to improve the resolution of linear features orientated parallel to the x-axis (Chambers et al., 2002; Gharibi and Bentley, 2005), and to improve the data density, and therefore resolution, within the area of most interest, i.e., the landfill and its western boundary. The along-line electrode separation was 5 m for all lines. All survey lines fell within the 3D electrical survey area shown on Figure 1 with the exception of the tie line at 120 m NE, which was extended northwards into the adjoining field. Data from this line were intended to provide additional information regarding potential bedrock contamination to the northwest of the landfill.

A prototype four-channel multi-electrode resistivity instrument capable of addressing up to 64 electrodes was used for data collection. A Wenner configuration was employed on one channel, but to make full use of the instrument and to improve lateral resolution, additional Schlumberger array configurations (Loke, 1999) were collected on the other

channels. These additional configurations were reciprocals of the traditional C-P-P-C arrangements (i.e. P-C-C-P, with the potential electrodes outside the Wenner current dipole). With the advent of multi-channel instruments the use of hybrid Wenner array types is becoming more common (e.g. de la Vega, 2003; Leucci et al, 2004; Zume et al, 2006) in order to harness the good signal strength of the Wenner array and the superior lateral resolution of other array types such as the dipole-dipole, Schlumberger and gradient arrays (Dahlin and Zhou, 2004). In this case a combination of Wenner and Schlumberger array configurations were selected to provide good lateral and vertical data coverage to a depth of approximately 30 m. Furthermore, the configurations had good signal to noise properties, and did not require the use of remote electrodes. The field survey was completed within a period of three days; measurement time, excluding setup and array deployment, amounted to 12 hours.

Numerical inversion

The 2D and 3D ERT field data were inverted using L_1-norm implementations (Loke and Lane, 2002) of the regularized least-squares optimization method (Loke and Barker, 1995 and 1996), based on the following equation:

$$\left(\mathbf{J}_i^{\mathrm{T}} \mathbf{R}_{\mathrm{d}} \mathbf{J}_i + \lambda_i \mathbf{C}^{\mathrm{T}} \mathbf{R}_{\mathrm{m}} \mathbf{C} \right) \mathbf{p}_i = \mathbf{J}_i^{\mathrm{T}} \mathbf{R}_{\mathrm{d}} \mathbf{g}_i - \lambda_i \mathbf{C}^{\mathrm{T}} \mathbf{R}_m \mathbf{C} \mathbf{g}_i \qquad (1)$$

where i is the number of iterations, $\mathbf{J}$ is the Jacobian matrix of partial derivatives, λ is the damping factor, $\mathbf{C}$ is the roughness filter matrix, $\mathbf{p}$ is the perturbation vector to the model parameters, $\mathbf{g}$ is the discrepancy (data misfit) vector that contains the difference between the logarithms of the measured and calculated apparent resistivity values, and $\mathbf{R}_{\mathrm{d}}$ and $\mathbf{R}_{\mathrm{m}}$ (Wolke and Schwetlick, 1988) are weighting matrices that are included so that different elements of the discrepancy and model roughness vectors are given equal weights during

the inversion. The forward problem was solved using the finite-element method, in which node positions were adjusted to allow topography to be taken into account in the inversion process (Loke, 2000). The measured dataset comprised approximately 7300 points collected from within the 3D survey area. The final 3D resistivity model consisted of 32 cells in x-direction, 42 cells in y-direction and 8 layers in the vertical direction, resulting in a total of 10416 model cells. Good convergence between the observed and model resistivity data was achieved after 6 iterations as indicated by an rms error misfit of 3.0 %. The inversion took approximately 8 hours to run on a AMD Athlon™, 2.41 GHz, machine with 2.0 GB of RAM.

The L_1-norm (robust) optimization method minimizes the sum of absolute values of the changes in model resistivity and was used in preference to the L_2-norm (smoothness constrained) method, which minimizes the sum of squares, as it provides significantly better results for situations where there are sharp boundaries (Loke et al., 2003). In this case it was important to determine the position of the boundaries between the resistive dolerite sill and more conductive units of the Upper Limestone formation and the highly conductive waste deposits. The superiority of the L_1-norm method for this type of problem is illustrated by Figure 3. The L_1- and L_2-norm optimization methods were each used to produce 3D models from the measured data. Figure 3a shows horizontal depth sections at 7.3 m bgl from the L_1- and L_2- norm models respectively. The dolerite / waste interface appears as a significantly better defined feature in the L_1-norm model. In Figure 3b, model resistivities coinciding with the location of intrusive sample point R02 were extracted from the 3D models and displayed as vertical plots alongside the geological log obtained from the borehole. The L_1-norm more closely reflects the abrupt change from the highly resistive dolerite to the more conductive underlying Upper Limestone Formation units shown in the corresponding geological log.

Interpretative criteria

The survey area includes a wide range of geological and man-made materials with greatly differing electrical properties. The dolerite sill is likely to be associated with the highest resistivities. Crystalline igneous rocks, such as quartz dolerite, are typically represented by resistivities of hundreds to tens of thousands of Ωm, depending on moisture content and degree of weathering (e.g., Telford et al., 1990). The Upper Limestone Formation in this area comprises mudstone, siltstone and sandstone; the resistivity of these materials will increase with increasing grain size and decreasing water content. Mudstones are expected to display resistivities of 10 to several tens of Ωm, whilst the sandstones may be characterized by resistivities from tens up to thousands of Ωm. The Quaternary sand and gravel to the north of the landfill is anticipated to display resistivities of a few tens to a few hundred Ωm, depending on moisture content.

Buried domestic waste is usually highly electrically conductive, with resistivities of less than 20 Ωm, particularly in water-saturated conditions where resistivities of less than 1 Ωm may occur (Ogilvy et al., 2002). The clay capping material is also likely to be characterized by low resistivities of less than 35 Ωm.

Pore fluid conductivity exerts a major influence on bulk material resistivity. Consequently, the migration of highly conductive landfill leachate in surrounding bedrock may be distinguished as a zone of low resistivity.

Integrated spatial modeling and visualization

Resistivity models resulting from numerical inversions are typically displayed as either 2D sections or 3D volumetric images. Beyond the display of physical property values alone, the calibration and interpretation of resistivity models requires spatial comparison

with reference data. To aid this process, relevant site investigation data and ground-truth information (Figure 2) has been integrated with the geophysical models in virtual 3D space using generic geological modeling software (Figures 4 and 5). Borehole logs in and around the survey area, the water table model, geophysical survey line positions, topographic surfaces and historic OS data have all been included along with the resistivity model in a dynamic 3D representation of the site.

Particular care was taken with the accurate visualization of the 3D resistivity model. Although spatial discretization of the subsurface for the purpose of inverse modeling is somewhat arbitrary, it is sensible and good practice to choose a mesh geometry that reflects the capabilities of the ERT method. Semi-automatic mesh generators employed by many popular ERT inversion algorithms fulfill these criteria. The resulting model grid is typically non-uniform and two key aspects of non-uniformity must be considered for the purpose of quantitative analysis and interpretation. Firstly, model layer thicknesses usually increase with depth to account for the loss in resolution away from the surface. Secondly, the effect of surface topography can be incorporated in the inversion process by means of a spatial transformation of the 3D finite-element grid. Hence the geometry of the resulting resistivity model is distorted accordingly and layers of cells conform to the surface topography over the entire vertical extent of the model. Visualization of such non-uniform model geometries can be achieved in advanced 3D geomodeling environments (Kuras, 2004). For presentation purposes, we have used Rockworks™ v.2004 to display the 2D and 3D resistivity models using a re-sampled grid with regular node spacings. In the case of the 3D model the re-sampled grid was generated using an inverse distance squared interpolation method in which a weighted average of the closest control point in each 90° sector around each node was calculated.

RESULTS AND INTERPRETATION

Model overviews

The 3D resistivity model includes resistivity values ranging from less than 1 Ωm to approximately 3000 Ωm. In order to accommodate the wide range of resistivities present, a logarithmic color scale has been used for visualization. The main features and components of the model are shown in Figures 4 and 5, which comprise 3D tomograms with opaque volumes showing resistivity distributions greater than 50 Ωm and less than 15 Ωm respectively.

A highly resistive zone, i.e. 10^2 to 10^3 Ωm, showing the extent of the dolerite sill covers much of the near surface of the model. The dimensions of this zone closely correspond to the thickness of the sill indicated by the borehole records, i.e. 10 to 15 m; moreover, the model resistivities are consistent with the high resistivities that are generally associated with dolerite. In the area of the model coinciding with the quarry, as shown by the intrusive and historic OS data, the resistive zone is absent, indicating the removal of dolerite. Towards the center of the survey area a resistive zone extends to the base of the model; this feature is shown in the northeast striking vertical sections in Figure 5. It is likely that this resistive feature is not a reflection of resistive material persisting to depth, but is instead due to a weakness of the inversion method and insufficient depth of investigation of the surface arrays. The lateral position of this resistive anomaly broadly coincides with an area of relatively conductive overburden above the sill. The greater depth to the base of the dolerite in this area is likely to have resulted in poorer resolution of the sill base, giving the appearance of high resistivities persisting below the sill. This hypothesis is supported by a 2D synthetic modeling study (Figure 6) designed to represent this situation, in which a dolerite sill with and without

conductive overburden is simulated (see Interpretative Criteria). In the case of overburden overlying the sill, the model produced from synthetic apparent resistivity data was unable to resolve the base of the sill. Instead the resistive zone representing the sill extended to the base of the model. Poor model resolution at the base of the buried sill is further confirmed by the sensitivity plot in Figure 6c; sensitivities are particularly low in the region of the buried sill due to current channeling in the conductive overburden.

The second dominant feature in the model is the conductive zone coinciding with the estimated location of the landfill. It is shown in blue on the vertical sections in Figure 4, and as a solid volume along the northeastern edge of Figure 5. A more resistive zone representing the clay capping materials and unsaturated waste overlies much of the conductive feature. Although a range of waste types with differing resistivities were disposed of at the site, the 3D ERT model shows relatively little variation within the area of the landfill. It is likely that this is due to mixing of leachate within the landfill, which has led to the homogenization of saturated waste resistivities. The western boundary of the quarry in particular appears in the model as a steep sided feature (Figure 4). Hard rock quarries are often steep sided due to the competent nature of the materials in which they are situated. Evidence from BH07 to BH07B and BH10A, which were located at the margins of the quarry, supports this observation.

A highly conductive anomaly at the base of the model can be seen in Figures 5 and 7 extending from 0 to 120 m NW along the southwestern model boundary. This anomaly appears to be unconnected to the landfill, and does not relate to any known feature associated with the site. The low resistivity values associated with this feature are lower than most natural occurring resistivities. Without further investigations it is impossible to identify the source of this feature. Given that it is located in a poorly constrained area of

the model and does not intersect any of the tie lines, it is likely that this feature is a spurious artifact of the inversion process.

Those areas of the model below the level of the dolerite sill and the landfill, which are characterized by resistivities ranging from approximately 10 to 200 Ωm, are likely to represent the sedimentary units of the Upper Limestone Formation.

The 2D model of the extended line 120 m NE is shown in Figure 8. Of most interest in this model is the area beyond 210 m NW, which is outside the area covered by the 3D survey. We consider the 3D model of the landfill to be inherently more reliable than the 2D model (e.g. Chambers et al., 2002; Bentley and Gharibi, 2004); discussion of the 2D model will therefore be limited to the area extending from 210 m NW. It can be seen that the conductive anomaly underlying the resistive surface zone is contiguous with the main conductive anomaly associated with the landfill and extends from approximately 160 to 230 m NW. An abrupt change to greater resistivities then occurs at this point, potentially indicating a fault controlled change to different units of the Upper Limestone Formation. Towards the end of the line, at Y = 276 m NE, a resistive zone is shown in the model. Borehole BH51 reveals the presence of dolerite to at least 13.9 m bgl at this location. Neighboring boreholes BH50 and BH52, in which no dolerite was observed, indicate that the dolerite in this area is not laterally extensive. It is likely the dolerite dike indicated on the geological map (Figure 1a) extends further to the east than originally predicted, and falls between boreholes BH50 and BH52.

Landfill boundaries and quarry spoil

The southwestern boundary of the landfill appears from the resistivity model to follow a line parallel to the *y*-axis at approximately 100 m NE. The boundary is seen in the near surface region of the model (i.e., Figure 7b) as a distinct feature, which corresponds

closely with the historic quarry boundary. Given the sharp contrast in the resistivity model, and the corroborative evidence provided by the historic OS data, the position inferred from the resistivity model is likely to be within a few meters of the landfill boundary; however, the accuracy of location of the boundary will not be better than the lateral resolution of the resistivity model. The resistivity model confirms that the edge of the landfill does not precisely follow the northwesterly striking topographic feature running across the survey area shown in Figure 1. As indicated by the historic OS data, the area of higher ground defined by approximately 50 to 100 m NE and 0 to 120 m NW has at the surface an area of made ground, up to 10 m thick, overlying bedrock. This surface layer is clearly defined and labeled in Figures 4 and 5, and is likely to consist of quarry spoil. It should also be noted that verification of the dolerite promontory extending from the southwestern edge of the quarry at approximately 20 m NW, as indicated by the historic boundary position, is provided in the resistivity model as a resistive anomaly extending into the quarry at this location (Figure 7a & b).

The change in physical properties representing the northwestern quarry boundary is located at approximately 160 m NW, though compared with the southwestern boundary it is a much more gradational feature (Figure 7). The electrically diffuse nature of this boundary may be a consequence of leachate infiltration into the bedrock.

Vertical landfill extent

Borehole data from the phase III site investigation indicates that the landfill deepens to the northwest. This is consistent with the historic OS data (Figure 2), which shows a haulage road leading from the quarry's southern end. The deepening of the landfill to the northwest is also seen in the resistivity model (Figure 9a). Borehole records (BH06, BH09 and BH11) from within the quarry area indicate that the maximum landfill depth is

likely to be approximately 14 to 15 m bgl. However, the conductive anomaly associated with the landfill includes resistivities of below 15 Ωm persisting to in excess of 25 m bgl, and has no distinct boundary corresponding to the landfill base. The apparent overestimation of landfill depth displayed by the resistivity model may be caused by leachate migration into underlying bedrock reducing the bedrock resistivities below the landfill. In addition, the appearance of greater depth is also likely to be a function of decreasing resolution with depth (Chambers et al., 1999; Olayinka and Yaramanci, 2000), as indicated by the very low model sensitivities in this region shown in Figure 9b.

The upper limits of the waste within the landfill are not immediately apparent from the resistivity images. However, the models do show a relatively resistive surface layer above the area of the landfill. This layer appears to fall at a similar level to model groundwater levels within the landfill at a depth of approximately 6 to 7 m (Figure 9a). Given that intrusive records for BH02 to BH11, and BH13 indicate the presence of a thin cap of only a few meters, it is clear that the more resistive zone at the surface is primarily a function of saturation state rather than material type.

Identification of potential leachate migration

The persistence of the conductive anomaly associated with the landfill to depths well below the landfill base provides evidence of leachate invasion into the underlying bedrock. However, the resolution towards the base of the model is relatively poor, and further groundwater sampling in the formations below the landfill is required to calibrate the model in this region.

Conductive anomalies associated with leachate migration from the southwestern quarry boundary are absent from the resistivity model. This finding is in keeping with the

groundwater level model (Figure 1b), in which groundwater flow along this boundary is shown to be moving into the landfill.

The anomalies with the greatest potential for association with leachate migration are those towards the northwestern boundary of the site. In particular, a conductive zone can be seen extending at depth from the landfill below the resistive surface layer in an area defined by 100 to 150 m NE and 160 to 205 m NW. This is potentially indicative of a zone of leachate migration to the northwest (Figure 7c). This conclusion is supported by evidence from borehole R02, in which several meters of sandstone were recorded below the sill in this area; sandstone would be expected to display a higher resistivity than that shown in the model at this location. Moreover, sandstone could have been exposed in the quarry, providing a more permeable pathway for leachate migration from the quarry. However, it is also possible that the sandstone is not laterally continuous and this conductive zone is associated with the presence of uncontaminated but relatively conductive Upper Limestone Formation strata, e.g., mudstone or siltstone units.

The 2D resistivity model provides no compelling evidence for leachate migration across the estimated location of the fault into the field directly to the northwest of the 3D survey area (Figure 8). Whilst it is conceivable that the fault could act as either a preferential pathway or barrier to groundwater flow, its influence on potential leachate migration pathways is not known.

CONCLUSIONS

Electrical imaging surveys have been undertaken at a former quarry and landfill site in the Midland Valley of Scotland. Data from these surveys have been modeled using 2D and 3D L1-norm inversion algorithms; the L1-norm method was shown to be preferable

to the L2-norm as it is better able to resolve sharp boundaries between materials with strongly contrasting resistivities, such as dolerite and domestic waste.

The landfill has been identified as a conductive feature, which closely coincides with the maximum extent of the quarry indicated by historic OS maps. The landfill base is seen in the resistivity models as a gradational interface extending far below the known base of the landfill. The low resistivity zone below the landfill base is indicative of leachate migration into the bedrock, though further groundwater sampling is required to confirm this hypothesis. Uncertainties and ambiguities associated with the interpretation of features at greater depth in the resistivity models (e.g. the landfill base) constitute a problem common to all ERT models generated from a surface electrode deployment, for which resolution decreases exponentially with depth, and reinforces the need for interpretation of such models to be carried out in conjunction with suitable ground-truth data.

A conductive zone, potentially indicating contaminated bedrock, extends from the northwestern landfill boundary in both the 2D and 3D resistivity models. Intrusive investigations have indicated that the direction of groundwater flow across this area of the site is approximately northwards, which supports the assertion that ERT has been effective in identifying a leachate plume emanating from the landfill.

Geological structures associated with the site, including the dolerite sill and dike, and the fault zones have been successfully imaged using ERT. The sill and dike were delineated as high resistivity features relative to the Upper Limestone Formation and the waste, whilst the fault zone was distinguished due to the contrasting resistivities of the Upper Limestone Formation on its upthrown and downthrown sides.

In this case the integrated use of ERT and conventional site investigation information coupled with the use of 3D visualization and analysis software has led to a far better

understanding of the site than could have been achieved using traditional site investigation methods alone.

ACKNOWLEDGEMENTS

REFERENCES

Abu-Zeid, N., G. Bianchini, G. Santarato, and C. Vaccaro, 2004, Geochemical characterisation and geophysical mapping of landfill leachates: the Marozzo Canal case study (NE Italy): Environmental Geology, **45**, 439-447.

Aristodemou, E., and A. Thomas-Betts, 2000, DC resistivity and induced polarisation investigations at a waste disposal site and its environments: Journal of Applied Geophysics, **44**, 275-302.

Bentley, L. R., and M. Gharibi, 2004, Two- and three-dimensional electrical resistivity imaging at a heterogeneous remediation site: Geophysics, 69, 674-680.

Bernstone, C., and T. Dahlin, 1997, DC resistivity mapping of old landfills: two case studies: European Journal of Environmental and Engineering Geophysics, **2**, 121-136.

Bernstone, C., T. Dahlin, T. Ohlsson, and W. Hogland, 2000, DC-resistivity mapping of internal landfill structures: two pre-excavation surveys: Environmental Geology, **39**, 360-371.

Binley, A., G. Cassiani, R. Middleton, and P. Winship, 2002, Vadose zone flow model parameterisation using cross-borehole radar and resistivity imaging: Journal of Hydrology, **267**, 147-159.

Cameron, I. B., and D. Stephenson, 1985, The Midland Valley of Scotland: British Regional Geology: HMSO.

Chambers, J. E., P. I. Meldrum, R. D. Ogilvy, and P. B. Wilkinson, 2005, Characterisation of a NAPL-contaminated former quarry site using electrical impedance tomography: Near Surface Geophysics, **3**, 79-90.

Chambers, J. E., R. D. Ogilvy, O. Kuras, J. C. Cripps, and P. I. Meldrum, 2002, 3D electrical imaging of known targets at a controlled environmental test site:

Environmental Geology, **41**, 690-704.

Chambers, J., R. Ogilvy, and P. Meldrum, 1999, 3D resistivity imaging of buried oil- and tar-contaminated waste deposits: European Journal of Environmental and Engineering Geophysics, **4**, 3-14.

Dahlin, T., C. Bernstone, and M. H. Loke, 2002, A 3-D resistivity investigation of a contaminated site at Lernacken, Sweden: Geophysics, **67**, 1692-1700.

Dahlin, T. and B. Zhou, 2004, A numerical comparison of 2D resistivity imaging with 10 electrode arrays, Geophysical Prospecting, **52**, 379-398.

Daily, W., A. Ramirez, and R. Johnson, 1998, Electrical impedance tomography of a perchloroethelyne release: Journal of Environmental and Engineering Geophysics, **2**, 189-201.

Daily, W., and A. L. Ramirez, 2000, Electrical imaging of engineered hydraulic barriers: Geophysics, **65**, 83-94.

de la Vega, M., A. Osella and E. Lascano, 2003, Joint inversion of Wenner and dipole-dipole data to study a gasoline-contaminated soil. Journal of Applied Geophysics, **54**, 97-109.

European Union (EU), 1999, Council Directive 1999/31/EC of 26 April 1999 on the landfill of waste: Official Journal of the European Communities, L 182/1 - L 182/19.

Francis, E. H., 1982, Magma, sediment - 1: emplacement mechanism of the late Carboniferous tholeiite sills in northern Britain: Journal of the Geological Society, **39**, 1-20.

Gharibi, M., and L. R. Bentley, 2005, Resolution of 3-D electrical resistivity images from inversions of 2-D orthogonal lines: Journal of Environmental and Engineering Geophysics, **10**, 339-349.

Goes, B. J. M., and J. A. C. Meekes, 2004, An effective electrode configuration for the detection of DNAPLs with electrical resistivity tomography: Journal of Environmental and Engineering Geophysics, **9**, 127-141.

Great Britain, 1974, Control of Pollution Act 1974: HMSO.

Guerin, R., M. L. Munoz, C. Aran, C. Laperrelle, M. Hidra, E. Drouart, and S. Grellier, 2004, Leachate recirculation: moisture content assessment by means of a geophysical technique: Waste Management, **24**, 785-794.

Kuras, O., 2004, Integrated 3D spatial modelling of electrical tomography data with GOCAD: IR/04/152R, British Geological Survey.

Leucci, G., S. Margiotta and S. Negri, 2004, Geophysical and geological investigations in a karstic environment (Salice Salentino, Lecce, Italy). Journal of Environmental and Engineering Geophysics, **9**, 25-34.

Loke, M. H., 1999, Electrical imaging surveys for environmental and engineering studies: A practical guide to 2-D and 3-D surveys, http://www.abem.se/files/res/2Dnotes.pdf, accessed June 6, 2006.

Loke, M. H., 2000, Topographic modelling in electrical imaging inversion: EAGE 62nd Conference and Technical Exhibition.

Loke, M. H., I. Acworth, and T. Dahlin, 2003, A comparison of smooth and blocky inversion methods in 2-D electrical imaging surveys: Exploration Geophysics, **34**, 182-187.

Loke, M. H., and R. D. Barker, 1995, Least-squares deconvolution of apparent resistivity pseudosections: Geophysics, **60**, 1682-1690.

Loke, M. H., and R. D. Barker, 1996, Practical techniques for 3D resistivity surveys and data inversion: Geophysical Prospecting, **44**, 499-523.

Loke, M. H., and J. W. Lane, 2002, The use of constraints in 2D and 3D resistivity modelling: 8th meeting of the European Section of the Environmental and Engineering Society, p. 4.

Meads, L. N., L. R. Bentley, and C. A. Mendoza, 2003, Application of electrical resistivity imaging to the development of a geologic model for a proposed Edmonton landfill site: Canadian Geotechnical Journal, **40**, 551-558.

Naudet, V., A. Revil, E. Rizzo, J. Y. Bottero, and P. Begassat, 2004, Groundwater redox conditions and conductivity in a contaminant plume from geoelectrical investigations: Hydrology and Earth System Sciences, **8**, 8-22.

Ogilvy, R., P. Meldrum, and J. Chambers, 1999, Imaging of industrial waste deposits and buried quarry geometry by 3-D resistivity tomography: European Journal of Environmental and Engineering Geophysics, **3**, 103-114.

Ogilvy, R., P. Meldrum, J. Chambers, and G. Williams, 2002, The use of 3D electrical resistivity tomography to characterise waste and leachate distributions within a closed landfill, Thriplow, UK: Journal of Environmental and Engineering Geophysics, **7**, 11-18.

Olayinka, A. I., and U. Yaramanci, 2000, Assessment of the reliability of 2D inversion of apparent resistivity data: Geophysical Prospecting, **48**, 293-316.

Reynolds, J. M., and D. I. Taylor, 1996, Use of geophysical surveys during the planning, construction and remediation of landfills, in S. P. Bentley, ed., Engineering Geology of Waste Disposal: London, The Geological Society, 93-98.

Sandberg, S. K., L. D. Slater, and R. Versteeg, 2002, An integrated geophysical investigation of the hydrogeology of an anisotropic unconfined aquifer: Journal of Hydrology, **267**, 227-243.

Telford, W. M., L. P. Geldart, and R. E. Sheriff, 1990, Applied geophysics: Cambridge University Press.

United States Environmental Protection Agency (USEPA), 1993, Criteria for solid waste disposal facilities - a guide for owners/operators: EPA/530-SW-91-089.

Walsh, D. C., and R. G. LaFleur, 1995, Landfills in New-York-City - 1844-1994: Groundwater, **33**, 556-560.

Williams, G. M., 1991, Landfill disposal of wastes, in R. A. Downing, and W. B. Wilkinson, eds., Applied Groundwater Hydrology: A British Perspective: Oxford, Oxford University Press, 114-133.

Williams, G. M., 1999, Natural attenuation of leachate - letting nature take its course (Reprinted from Trans. Instn. Min. Metall., vol 108, 1999), **108**, B33-B37.

Wolke, R., and H. Schwetlick, 1988, Iteratively reweighted least-squares - algorithms, convergence analysis, and numerical comparisons: SIAM Journal of Scientific and Statistical Computations, **9**, 907-921.

Yoon, J. R., K. Lee, B. D. Kwon, and W. S. Han, 2003, Geoelectrical surveys of the Nanjido waste landfill in Seoul, Korea: Environmental Geology, **43**, 654-666.

Yuval, and D. W. Oldenburg, 1996, DC resistivity and IP methods in acid mine drainage problems: results from the Copper Cliff mine tailings impoundments: Journal of Applied Geophysics, **34**, 187-198.

Zume, J, T, A. Tarhule and S. Christenson, 2006, Subsurface imaging of an abandoned solid waste landfill site in Norman, Oklahoma. Ground Water Monitoring & Remediation, **26**, 62–69.

LIST OF FIGURES

array, identical to that used for the field survey, and (c) the model sensitivity

distribution calculated from the Jacobian matrix for the last iteration.

Figure 7. Horizontal depth sections through the 3D model at (a) 80, (b) 75, (c) 67.5 m

and (d) 57.5 m above datum respectively.

Figure 8. 2D resistivity model, with an rms error of 2.3 %, generated from extended

survey line $x = 120$ m NE (Figure 1). The explanation for the borehole log is

given in Figure 2.

Figure 9. (a) 2D section through the 3D resistivity model at $x = 120$ m NE. The

groundwater model is shown as a dashed black line, and the estimated quarry

geometry is shown by the dashed white line. The explanation for the borehole

log is given in Figure 2. (b) Sensitivity section without topography, at $x = 120$

m NE, calculated from the Jacobian matrix for the last iteration of the 3D

inversion.
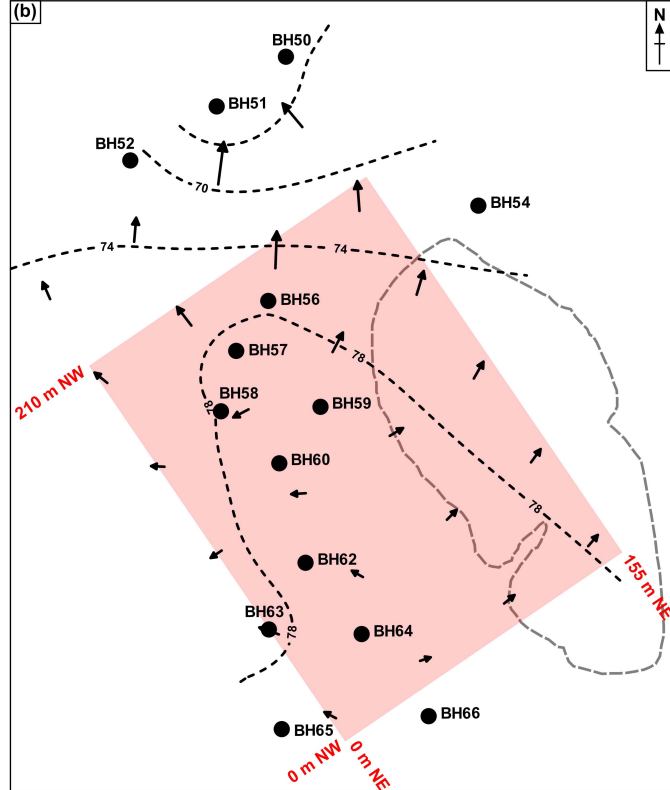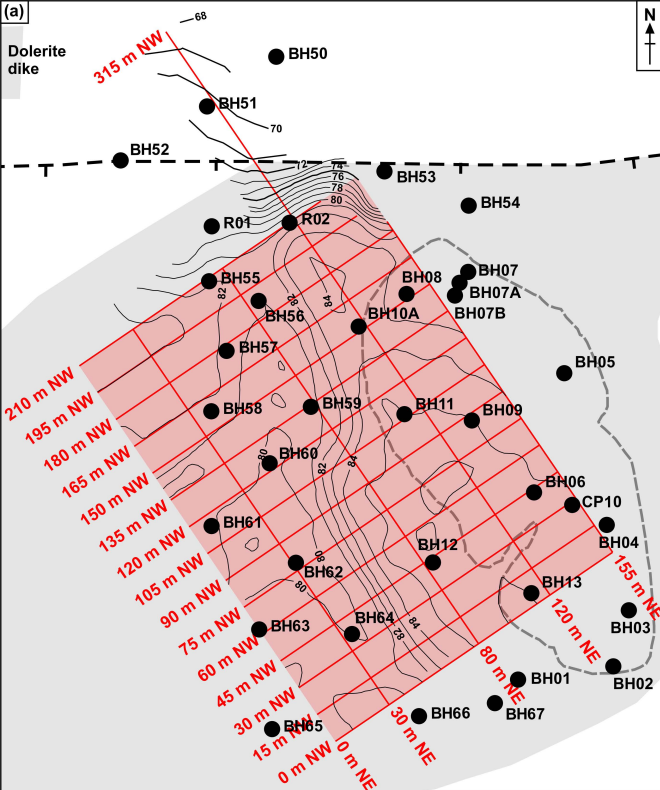
EXPLANATION

- ▬▬T Fault, crossmark on downthrown side
- Quartz-dolerite; intrusive
- Upper Limestone Formation
- ⌐68⌐ Topographic contour (metres above datum)
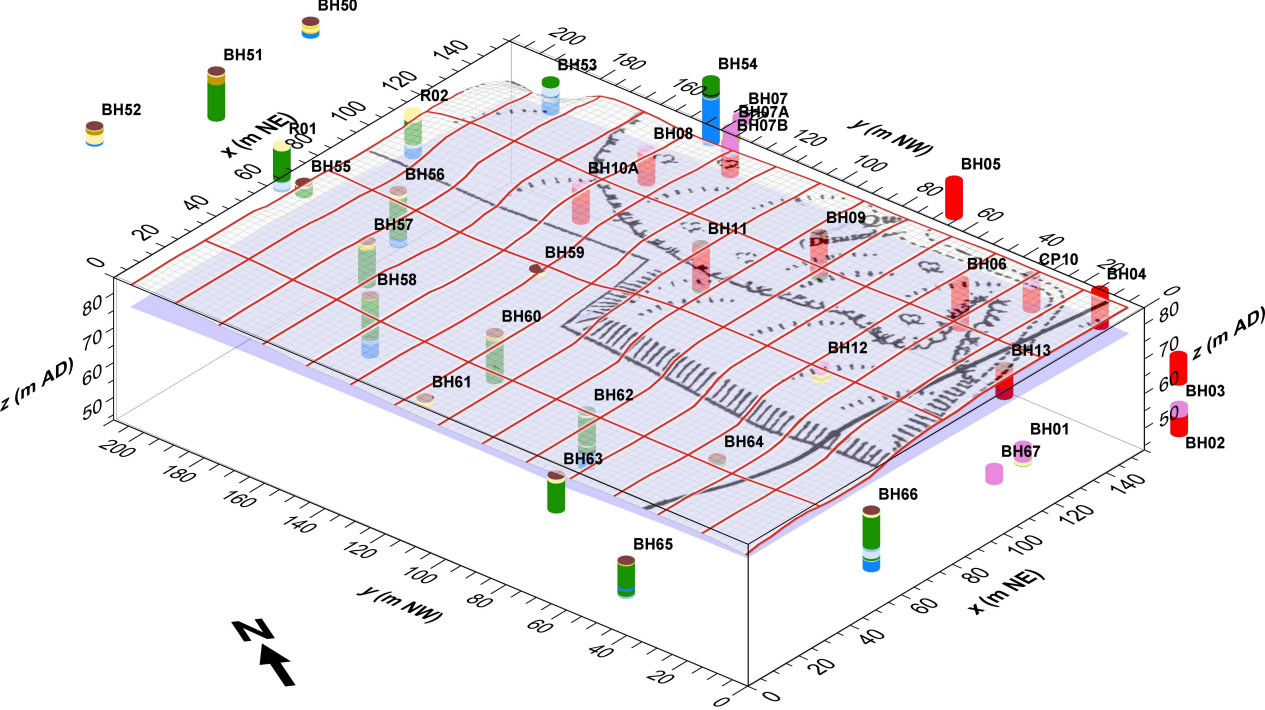- 3D electrical survey area
- ▬ Electrical survey line
- ● Borehole / trial pit
- ⌐ ⌐ Quarry outline (c.1950)
- ⌐77⌐ Water level contour (metres above datum)
- ↗ Groundwater flow line

Figure 1

Explanation

Made Ground

Waste

Topsoil

Dolerite

Calcite Vein

Drift
- Peat
- Clay
- Silt
- Sand
- Gravel
- Sand and Gravel

Upper Limestone Formation
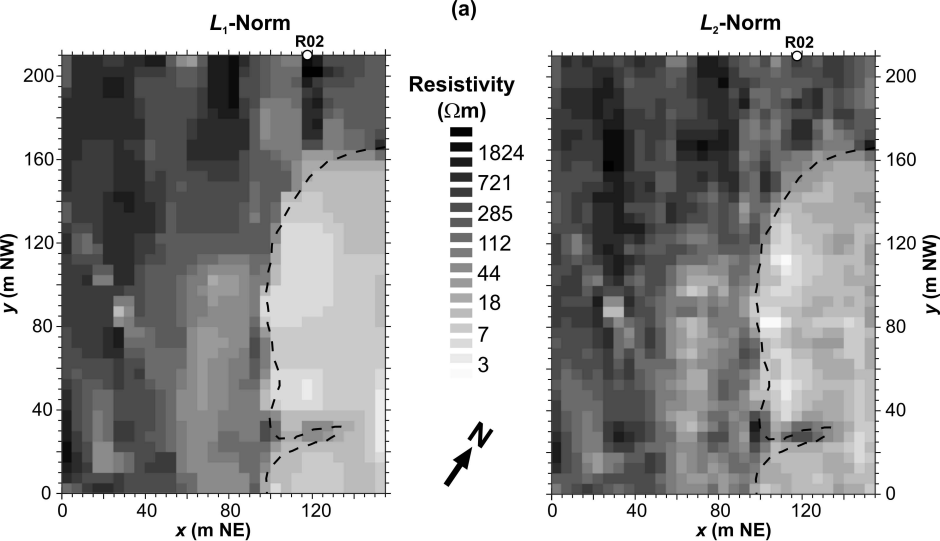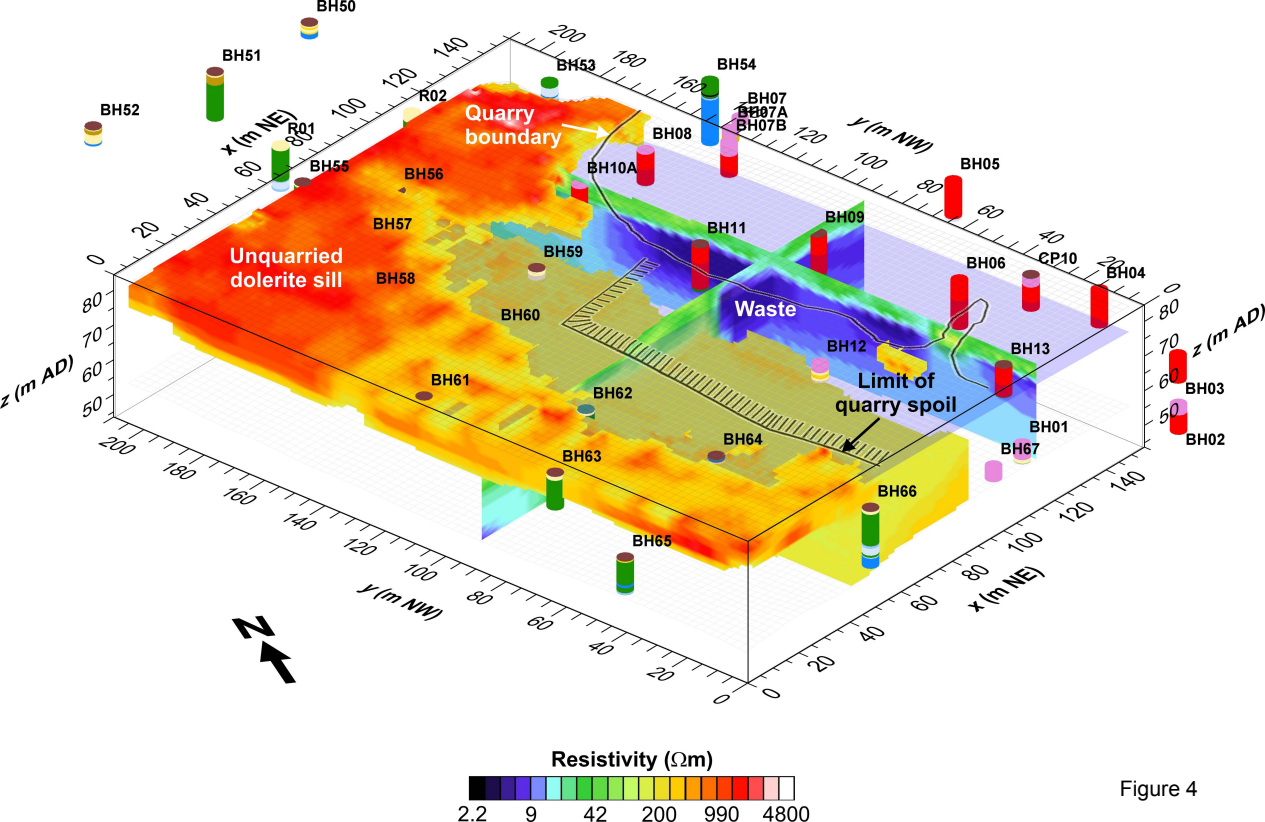- Mudstone
- Siltstone
- Sandstone
- Seatclay
- Coal

Figure 2

(a)
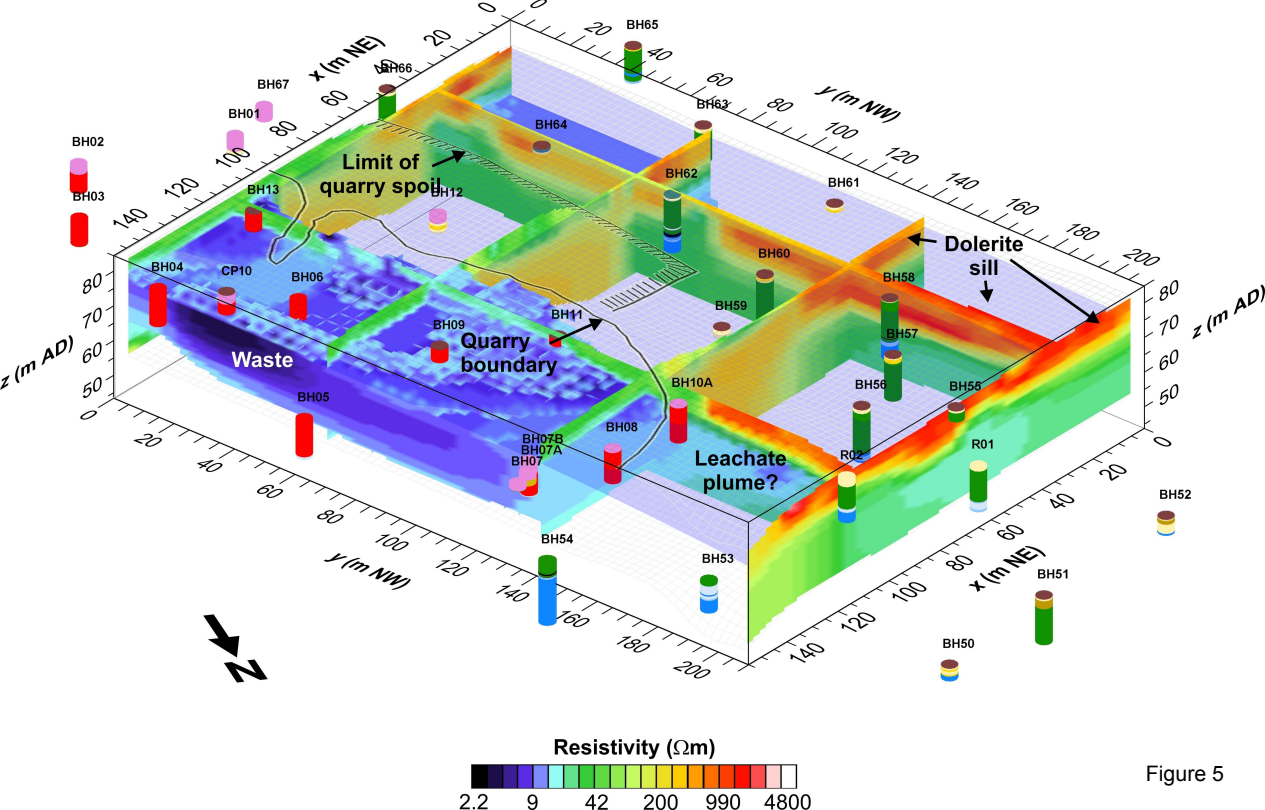
L_1-Norm

L_2-Norm

Resistivity (Ωm)

1824
721
285
112
44
18
7
3

(b)

R02

Key
- Dolerite
- Sandstone
- Siltstone
- Mudstone
- Clay/topsoil
- Coal
- ▽ Water level
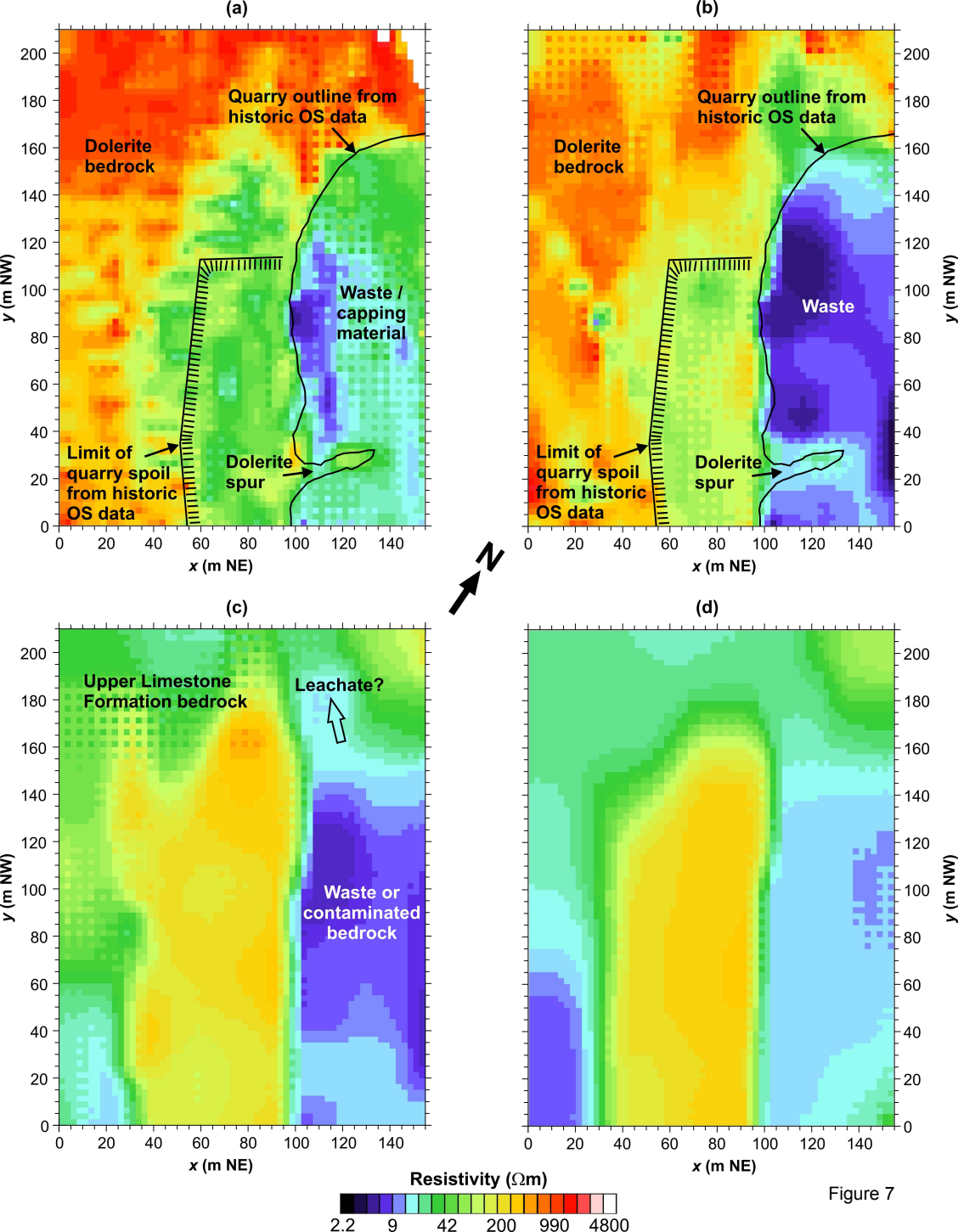- —— L_1-norm model resistivity
- —— L_2-norm model resistivity

Figure 3

Figure 4

Figure 5

(a)

| 750 Ωm (dolerite sill) | 35 Ωm (overburden) |
| 70 Ωm (mudstone) | 750 Ωm (dolerite sill) |

(b)

Resistivity (Ωm)

19   67   238   837

(c)

Sensitivity

0.04   0.20   1.1   6.0

Figure 6

(a)

Quarry outline from historic OS data

Dolerite bedrock

Waste / capping material

Limit of quarry spoil from historic OS data

Dolerite spur

(b)

Quarry outline from historic OS data

Dolerite bedrock

Waste

Limit of quarry spoil from historic OS data

Dolerite spur

(c)

Upper Limestone Formation bedrock

Leachate?

Waste or contaminated bedrock

(d)

N

y (m NW)

x (m NE)

Resistivity (Ωm)

2.2　9　42　200　990　4800

Figure 7

Figure 8

(a)

(b)

Figure 9